Journal of Power Sources 196 (2011) 8031–8040

Contents lists available at ScienceDirect

Journal of Power Sources

journal homepage: www.elsevier.com/locate/jpowsour

Two-phase flow pressure drop hysteresis in an operating proton exchange membrane fuel cell

Ryan Anderson [a,b], David P. Wilkinson [a,b,*], Xiaotao Bi [a,b], L. Zhang [a,b]

[a] Department of Chemical and Biological Engineering, University of British Columbia, 2360 East Mall Vancouver, BC, Canada V6T 1Z3
[b] Clean Energy Research Centre, University of British Columbia, 2360 East Mall Vancouver, BC, Canada V6T 1Z3

ARTICLE INFO

Article history:
Received 14 February 2011
Received in revised form 13 May 2011
Accepted 19 May 2011
Available online 27 May 2011

Keywords:
Two-phase flow
Hysteresis
PEM fuel cell
Water management

ABSTRACT

Two-phase flow pressure drop hysteresis was studied in an operating PEM fuel cell. The variables studied include air stoichiometry (1.5, 2, 3, 4), temperature (50, 75, 90 °C), and the inclusion of a microporous layer. The cathode channel pressure drops can differ in PEM fuel cells when the current density is increased along a path and then decreased along the same path (pressure drop hysteresis). Generally, the descending pressure drop is greater than the ascending pressure drop at low current densities (<200 mA cm^{-2}), and the effect is worse at low stoichiometries and low temperatures. The results show that the hysteresis occurs with or without the inclusion of a microporous layer. Initial results show a modified Lockhart–Martinelli approach seems to be able to predict the two-phase flow pressure drop during the ascending path. The results compare well with photographs taken from the cathode flow field channel of a visualization cell.

1. Introduction

The proton exchange membrane fuel cell (PEMFC) has received attention as an energy conversion device due to its high energy efficiency, low operating temperature, and little to zero emissions during operation. Though a promising technology, several issues impede the use of fuel cells in practical applications. One such technical issue that has received extensive research is proper water management. A specific consideration receiving additional attention recently is the impact of gas–liquid two-phase flow in the gas flow channels [1]. Two-phase flow in PEM fuel cells is a complicated phenomenon, requiring additional studies for a comprehensive understanding of water management [2,3].

Two-phase flow in PEM fuel cells is a unique multiphase flow due to large gas to liquid ratios, water produced by electrochemical reaction, and water condensing in the flow channels from humidified reactants and other operating conditions. Another important distinction is that water is introduced into the air flow field channels from a porous gas diffusion layer (GDL) instead of each phase being introduced together via a common inlet. Furthermore, the coupled gas and liquid flow rates (via Faraday's law) and the contact angles of each wall (flow field walls and GDL in the same channel) make two-phase flow studies in PEM fuel cells a challenge. Liquid water in flow channels can cause channel blockage, which can increase the pressure drop in the channel, and formation of a liquid film on the GDL surface, which blocks the reactant gas from reaching active catalyst sites. Experiments have shown the following flow patterns in parallel cathode flow field channels: slug, film, corner, and mist flow [4]. Film flow is considered a desirable flow pattern for water removal in fuel cells due to water traveling on the sidewalls instead of the GDL surface [2]. However, a specific combination of surface properties and superficial gas and liquid velocities must be met in order to ensure the desired pattern. Parallel channels have shown the potential for high performance when no flooding occurs, but this flow field configuration is flooding prone and more research is needed for improved water management [5].

A recently studied two-phase flow phenomenon is pressure drop hysteresis [6–9]. This behavior occurs when the gas and liquid flow rates (determined by a given current density) are increased along a set path and then decreased along the same path with differing pressure drops. An application exhibiting increasing and decreasing currents is the automobile, where the load varies based on the driving cycle [10,11]. Additionally, flow regime hysteresis has been observed in minichannels bounded by a porous wall, where the transition between flow regime depended on whether the air flow rate was varied in an ascending or descending manner [12]. However, these studies were accomplished in non-operating fuel cells. A higher pressure drop represents a larger system parasitic power loss [13], thus the hysteresis phenomenon requires additional study. Another problem associated with two-phase flow

* Corresponding author at: Department of Chemical and Biological Engineering, University of British Columbia, 2360 East Mall Vancouver, BC, Canada V6T 1Z3. Tel.: +1 604 822 4888; fax: +1 604 822 6003.
E-mail addresses: dwilkinson@chml.ubc.ca, dwilkinson@chbe.ubc.ca (D.P. Wilkinson).

0378-7753/$ – see front matter © 2011 Elsevier B.V. All rights reserved.
doi:10.1016/j.jpowsour.2011.05.050

Nomenclature

C	Chisholm parameter
i	current density, A cm^{-2}
$\dot{m}$	mass flow rate, g s^{-1}
ΔP	pressure drop, Pa
T	temperature, K
u	superficial velocity, m s^{-1}
V	voltage, V

Greek letters

λ_i	stoichiometric ratio of gas i
φ	two-phase flow multiplier
χ^2	Martinelli parameter
μ	viscosity (Pa s)

Subscripts

air,needed	required air demand at a given current density
air,supplied	supplied air at a given current density
↑↓	ascending and descending, respectively
2-phase	two-phase system, liquid water/gas
1-phase	single-phase system, gas only
g	gas
L	liquid
gl	gas and liquid together, two-phase flow
x	distance from channel inlet

and liquid water in flow channels is reactant maldistribution [14] and current maldistribution [15], which can lower overall cell performance.

This paper explores pressure drop hysteresis in an operating fuel cell at practical fuel cell operating conditions. Variables studied include the air stoichiometry, temperature, and inclusion of a microporous layer (MPL). The temperature [16–18], GDL properties [19–21], and air stoichiometry [16,17,22,23] were chosen for investigation due to their relevance to fuel cell performance [16,19–22] and two-phase flow pressure drop [17,18,23,24]. Finally, an empirical approach to predicting the two-phase pressure drop based on the Lockhart–Martinelli approach is presented.

2. Experimental methods

A visualization fuel cell was utilized to observe two-phase flow in the cathode flow field channels. The anode and cathode flow fields consisted of four parallel channels, 1 mm × 1 mm in cross-section and 30 cm long. The cathode flow channels were fabricated through a 1 mm thick stainless steel plate, which was then gold coated. These materials are typical of visualization fuel cells [1]. The landing widths are 1 mm and the fuel cell active area is 35.7 cm^2. An optically clear manifold allowed for direct observation into the cathode flow field channels. Extension areas on each flow field plate allowed for heating via Kapton heaters (Omega KH Series). The cell was compressed to 620 kPag. Schematics of the visualization cell have been published previously [6].

A Hydrogenics^{TM} test station (Model no. G100) was used to control and measure relevant operating variables including the air and hydrogen flow rate, operating temperatures, the load, and the voltage. Omega 164PC01D37 pressure transducers (0–2500 Pa) separate from the test station were used to measure the cathode flow channel's pressure drop. A Pixelink PL-A774 camera with an Edmund Optics VZM 300 lens and a MI-150 high intensity illumination system was used to capture images of the two-phase flow. The experimental setup is shown schematically in Fig. 1.

Table 1
Baseline conditions for all relevant operating variables.

Operating variable	Baseline value
T_{cell}, T_{gas}, $T_{dew\ point}$	75 °C
Relative humidity (cathode and anode)	100%
Cathode GDL	SGL Carbon 25 BC
Anode GDL	SGL Carbon 25 DC
Catalyst coated membrane (Pt loading)	Gore Primea Series 5510 (0.4 mg Pt cm^{-2})
Air stoichiometry (λ_{air})	2
H_2 stoichiometry	1.5
Cathode gas	Air
Flow fields	4 parallel, square channels
Compression pressure	620 kPag
Gas backpressure	206.8 kPag

The minimum air flow rate is determined from Faraday's law, but the stoichiometry, which is defined as the ratio of reactant supplied to the minimum reactant flow needed for the reaction to proceed, is utilized (Eq. (1)).

$$\lambda_{air} = \frac{\dot{m}_{air,supplied}}{\dot{m}_{air,needed}} \quad (1)$$

The current density, i, was run in an ascending manner and then in a descending manner to determine the extent of hysteresis in the pressure drop. The term ascending approach describes the path by which the current density was increased, which was as follows: 50, 100, 200, 400, 600, 800, 1000 mA cm^{-2}. The descending approach was this path in reverse. The single-phase pressure drop at each condition is the gas flow only pressure drop where the fuel cell is held at the open circuit voltage and the gas flow rate is increased in accordance with Faraday's law and the stoichiometry at each current density. Each current density was held for approximately 10 min. The voltage signal was sampled at 1 Hz and the pressure drop data was sampled at 20 Hz. The gas inlet and outlet lines were insulated and dry gas was used between trials to remove excess water and ensure a dry initial condition. The results presented are an average of three trials at each set of conditions and indicate that good repeatability was achieved. Examples of the standard deviation from three trials for the pressure drop measurements are shown in Figs. 2a and 4b, and for the electrochemical performance are shown in Fig. 10b.

The relevant baseline conditions for all operating variables are listed in Table 1. The temperatures studied are 50, 75, and 90 °C and the air stoichiometries studied are 1.5, 2, 3, and 4. These operating conditions are in a narrow range relevant to PEM fuel cells as defined by the US Fuel Cell Council [25]. The gas diffusion layers with their relevant specifications are provided in Table 2. The SGL 25 BC and 25 BA GDLs were chosen to study the impact of an MPL on hysteresis. The SGL 25 DC GDL is used on the anode side for all experiments.

3. Experimental results and discussion

Pressure drop data and polarization curves are presented for the variables studied. It should be noted that while the ascending and descending approaches show differences in pressure drop, the electrochemical performance in either approach is generally within 10 mV at a given current density. Thus, only the ascending

Table 2
Gas diffusion layers and specifications.

Company	GDL	MPL	PTFE content	Thickness (μm)
SGL Carbon	25 BC	Yes	5%	235
SGL Carbon	25 BA	No	5%	190
SGL Carbon	25 DC	Yes	20%	231

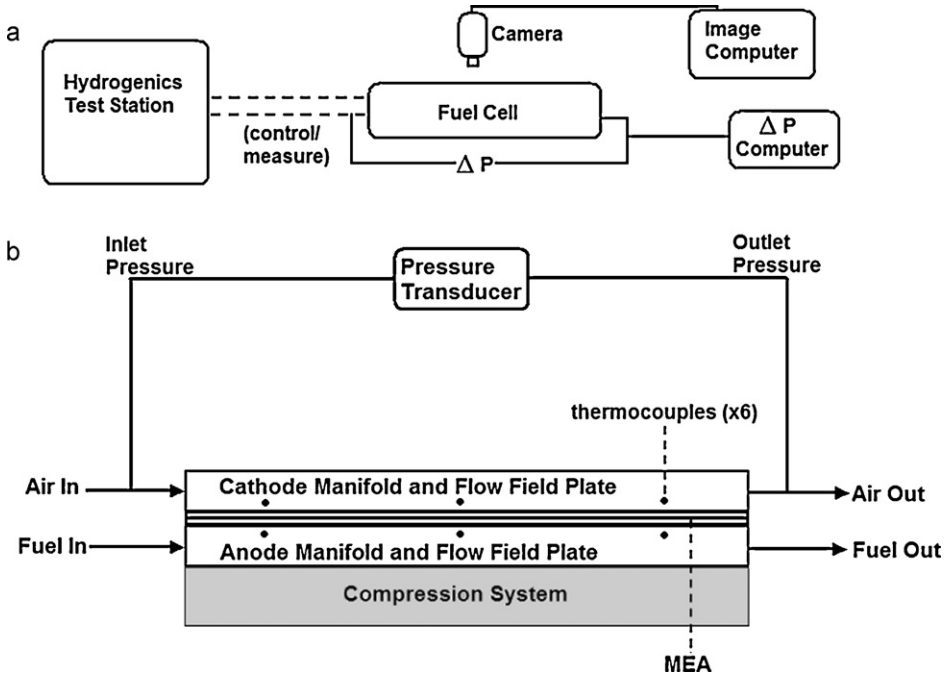

Fig. 1. (a) General data acquisition schematic; (b) cathode flow ΔP schematic.

approaches of the electrochemical polarization curves are presented for clarity unless otherwise noted. Also, in the visualization cell, the limiting current is approached or reached at approximately 1000 mA cm^{-2}, leading to low repeatability and accuracy at these points. These data points are included only to indicate that the fuel cell has reached the limiting current density. These results also indicate that this fuel cell performs as well as or better than other visualization cells with parallel channels in the literature [16], where it is noted that visualization cells have lower performance than traditional fuel cells [5]. Since the transparent fuel cells allow direct observation of the water in the cathode channels, the reduction in performance toward higher current densities is considered acceptable.

3.1. Causes of pressure drop hysteresis

Pressure drop hysteresis results for air stoichiometry 1.5 are shown in Fig. 2a. The highlighted area focuses on the hysteresis, where the descending pressure drop is higher than the ascending pressure drop at current densities <200 mA cm^{-2}. The magnitude of the pressure drop is consistent with fuel cell literature for parallel channels [5,26]. Fig. 2b shows the ratio of the descending pressure drop to the single-phase pressure drop at all stoichiometries studied and at each current density. The fitted curve is provided for visualization purposes. It is apparent that there is a sharp increase in pressure drop at lower current densities and stoichiometries. The pressure drop behavior is important at lower current densities because low loads are often used for high energy conversion efficiency [27] and dynamic automotive fuel cells often operate at less than 20% of the rated power, making the regime of lower gas flow important [28].

At this air stoichiometry, the two-phase pressure drop in both the ascending and descending approach is higher than the single-phase pressure drop at current densities ≥200 mA cm^{-2}. Also, at i > 200 mA cm^{-2}, the ascending and descending approach exhibit similar behavior, meaning that there is similar two-phase behavior in either approach. However, below 200 mA cm^{-2}, the descending pressure drop is noticeably higher at the lower stoichiometry due to more liquid water accumulating in the descending approach. Water enters the flow field channels via two mechanisms: (i) liquid water breakthrough from the GDL and (ii) humidified gas condensation. Condensation is a particular problem since the rate of condensation is much greater than the rate of evaporation when the gas stream is fully humidified [29]. These relative rates of

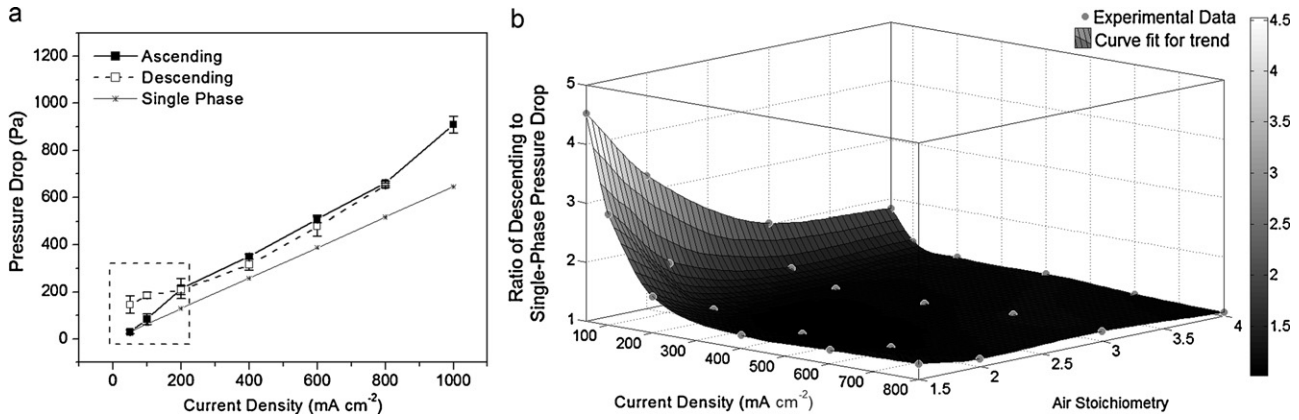

Fig. 2. (a) ΔP hysteresis curves for λ_{air} = 1.5; (b) ratio of the descending pressure drop to single-phase pressure drop at λ_{air} = 1.5, 2, 3, 4 for all current densities.

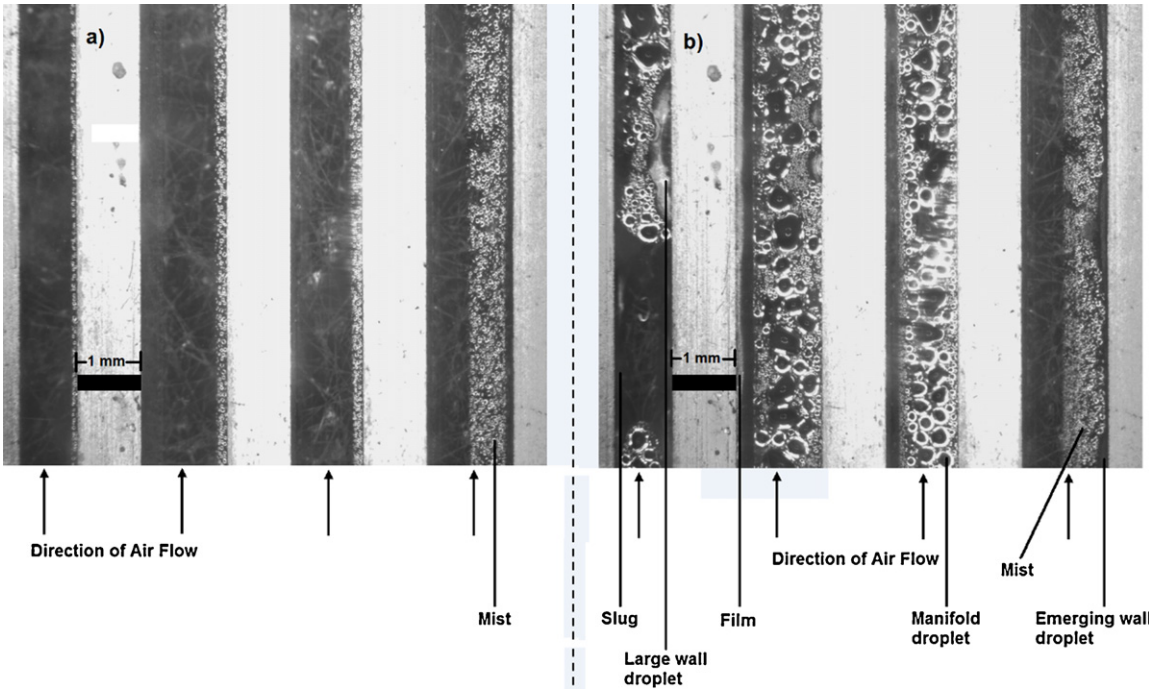

Fig. 3. (a) Cathode flow channels at 50 mA cm^{-2} for an ascending path; (b) cathode flow channels at 50 mA cm^{-2} for a descending path; λ_{air} = 1.5 with all other conditions at the baseline.

evaporation and condensation mean the liquid water must be removed convectively.

The hysteresis highlighted in Fig. 2a can be explained by an accumulation of liquid water in the descending approach that is greater than the accumulation in the ascending approach. Water accumulation during the ascending and descending approaches at 50 mA cm^{-2} at baseline conditions is shown in Fig. 3a and b, respectively. The same location is photographed in both approaches at the channels' exit. In the ascending approach, the only two-phase flow pattern is a mist flow that develops on the manifold surface (top wall). In the descending approach, accumulated liquid water led to a combination of slugs, films, wall droplets, and manifold droplets. It is also interesting to note that these descending flow patterns vary with channel, indicative of two-phase flow maldistribution. The increased flooding causes an increase in the pressure drop, resulting in ΔP hysteresis. Spernjak et al. [5] found a similar flooding mechanism in parallel channels via neutron imaging, where stationary droplets grew over time to form slugs before expulsion. Cathode water accumulation is also noted by Kimball et al. [30] when the cathode is facing 'up', where gravity acts to pull the droplet onto the GDL perpendicular to the direction of flow. By a similar mechanism, the slightly higher ascending pressure drop (at 400 and 600 mA cm^{-2}) is likely due to some water condensation at the lower flow rates. This water is convectively removed by higher air flow rates later in the ascending approach (800 mA cm^{-2}) and does not re-accumulate in the descending approach at the moderate to high current densities (at $i \geq 400$ mA cm^{-2} the higher flow rates are less prone to this condensation and accumulation).

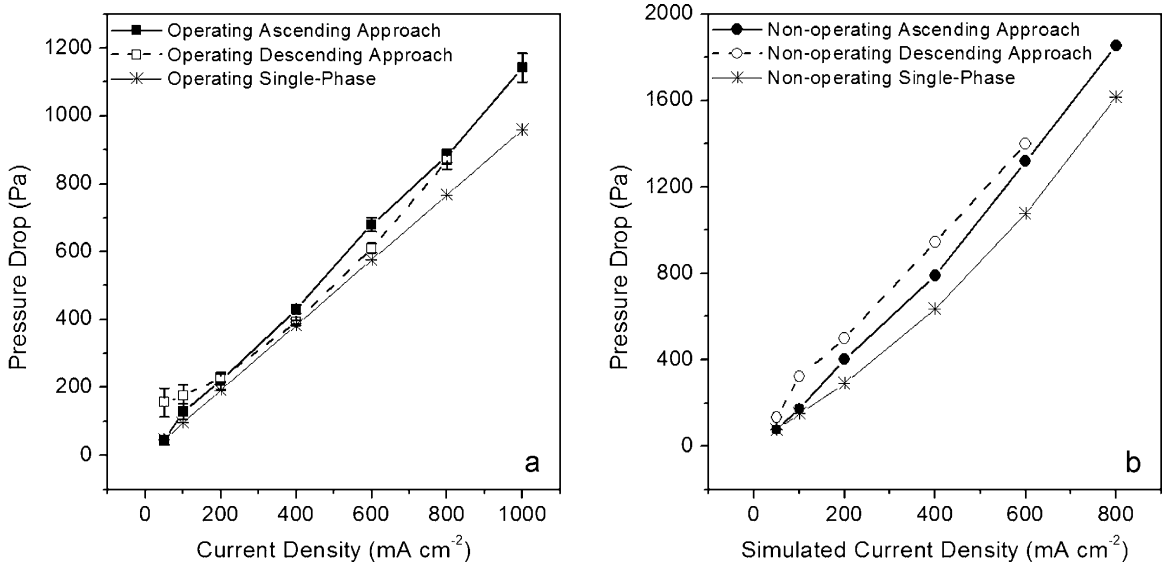

Fig. 4. Pressure drop hysteresis curves at the baseline conditions for (a) the operating fuel cell (baseline conditions from Table 1); (b) a non-operating fuel cell (T = 75 °C, RH = 100%, GDL = SGL 25 BC, P_{gas} = 0 kPag).

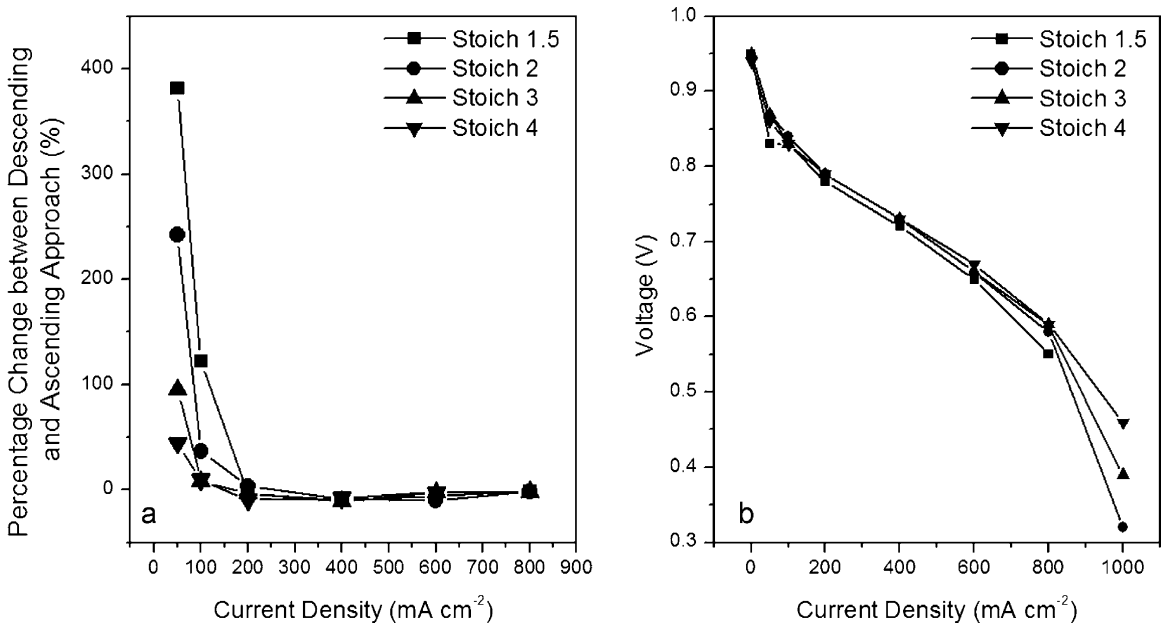

Fig. 5. (a) Percentage change between descending and ascending ΔP for λ_{air} = 1.5, 2, 3, 4; (b) ascending polarization curves for λ_{air} = 1.5, 2, 3, 4.

The mechanism described here qualitatively matches our experimental results from a non-operating study [6,9]. A comparison between the current operating study and the non-operating fuel cell results [9] are shown in Fig. 4a and b, respectively. Both experiments are with the 25 BC GDL at 75 °C with fully humidified air and an air stoichiometry of 2. However, in the non-operating case, the pressure is ambient (vs. 206.8 kPag in the operating cell) and water was injected externally into the cathode to simulate water production under the assumption that all of the water would enter the cathode. As that assumption is removed in the operating fuel cell, the hysteresis zone changes but is still a relevant consideration. In the non-operating case, the overall pressure drop increases due to the increased gas velocity (no backpressure) and all the water entering the cathode flow field channel. GDL saturation and water breakthrough dynamics can also be alerted in the non-operating case since electrochemically produced water is distributed with the current distribution. Also in the operating cell, water can move toward the anode, which limits the amount of water entering the cathode, reducing the impact of two-phase flow. However, this transport mechanism is likely small when both anode and cathode gas streams are fully humidified. Thus, in fuel cells experiencing little anode water removal, cathode pressure drop hysteresis may be a greater concern.

These results are also relevant to fuel cells with typical graphite bipolar plates. The water emerging from the hydrophobic GDL surface can spread to the hydrophilic walls as shown in Fig. 3b. In this study, the contact angles of the gold-coated flow field plates and the clear manifold are both ~60°. These values are comparable to typical graphite plates where the contact angle is between 70° and 80° [31], with some experimental graphite plates measured lower

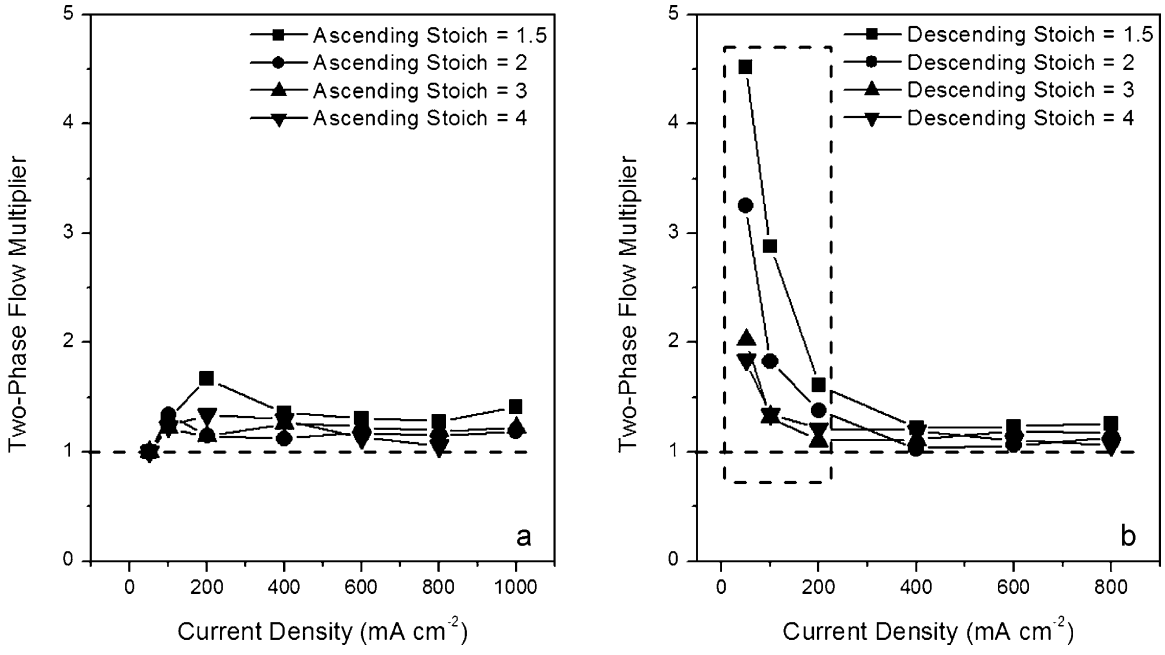

Fig. 6. Two-phase flow multiplier for air stoichiometries of 1.5–4 for (a) the ascending approach and (b) the descending approach.

at 46° [32]. Graphite plate fuel cells thus approximately match the wetting properties of the experimental apparatus utilized in this study.

3.2. Effect of stoichiometry

The additional accumulation of water between descending and ascending approaches depends on the ability of the air to convectively remove the liquid water, which is dependant on the gas velocity and therefore gas stoichiometry. Air stoichiometries of 1.5, 2, 3, and 4 were studied as practical fuel cell stoichiometries. The remaining operating conditions were set to the baseline conditions described in Table 1. To gauge the extent of the hysteresis, the percentage change between the descending and ascending approach is used, which is defined for a given current density as:

$$\%\text{Change}_{\uparrow,\downarrow} = \frac{\Delta P_{\text{Descending},i} - \Delta P_{\text{Ascending},i}}{\Delta P_{\text{Ascending},i}} \times 100 \quad (2)$$

The results of this analysis are shown in Fig. 5a along with the electrochemical performance results shown in Fig. 5b. The ΔP hysteresis is clearly noted at current densities <200 mA cm^{-2}. In this region, the percentage change between approaches is most noted for the lowest stoichiometry, 1.5, and is reduced with each increase in air flow rate. The increasing air flow rate (and therefore increasing convective water removal ability) allows less accumulation of liquid water in the descending approach, causing the hysteresis to diminish. A percentage change less than zero (200–600 mA cm^{-2}) indicates the descending pressure drop is lower than the ascending pressure drop, which is the result of slight condensed water accumulation on the ascending approach that is subsequently removed before the descending approach. However, this is a minor effect compared to the lower current densities.

The two-phase flow multiplier provides useful insight into the magnitude of the hysteresis and the general impact of the two-phase flow pressure drop. The two-phase flow multiplier, φ, is defined as:

$$\varphi_{\text{2-phase}} = \frac{\Delta P_{\text{2-phase}}}{\Delta P_{\text{1-phase}}} \quad (3)$$

A ratio of 1 means the ascending or descending approaches have the same pressure drop as the single-phase pressure drop, i.e., there is no influence of the liquid water. The two-phase flow multiplier for the ascending and descending approaches is highlighted in Fig. 6a and b, respectively. The ascending approach highlights the increased pressure drop due to two-phase flow, meaning that the product water and condensation are increasing the pressure drop. This influence is seen at all stoichiometries, which implies that the product water represents an inevitable parasitic power loss for the system due to an increased pressure drop. The descending approach two-phase flow multiplier shows a large increase in the multiplier in the hysteresis zone (<400 mA cm^{-2}). As discussed, it is at these lower current densities where additional water accumulates since the low air flow cannot convectively remove the liquid water. This effect is worse at lower stoichiometries and is lessened as the stoichiometry of the air (and therefore convective removal ability) increases. The descending two-phase multiplier is also shown in Fig. 2b for describing the general mechanism of pressure drop hysteresis.

In addition to larger pressure drop hysteresis, the fuel cell does not perform as well electrochemically at an air stoichiometry of 1.5 compared to higher stoichiometries. The lower performance is further exacerbated by voltage signal fluctuations at low current densities, which improve with increasing air stoichiometry as shown in Fig. 7. The voltages signals at 100 mA cm^{-2} are shown in Fig. 7 for the stoichiometries studied.

3.3. Effect of temperature

The pressure drop hysteresis and cell performance were measured at 50, 75, and 90 °C. All other operating conditions were set to the baseline conditions in Table 1. The percentage change between the descending and ascending approaches at these temperatures and the electrochemical performance are shown in Fig. 8a and b, respectively. It should be noted that at high current densities (around 1000 mA cm^{-2}) the voltage oscillations were very large and not every trial was able to sustain the voltage. Thus, the accuracy of these high current density values is reduced and the data is shown only to point out the limiting current density behavior.

The lowest temperature has the highest extent of hysteresis, and the hysteresis is reduced with increasing temperature until at 90 °C there is little hysteresis. These results are due to the increased air velocity at higher temperatures, which results in higher convective

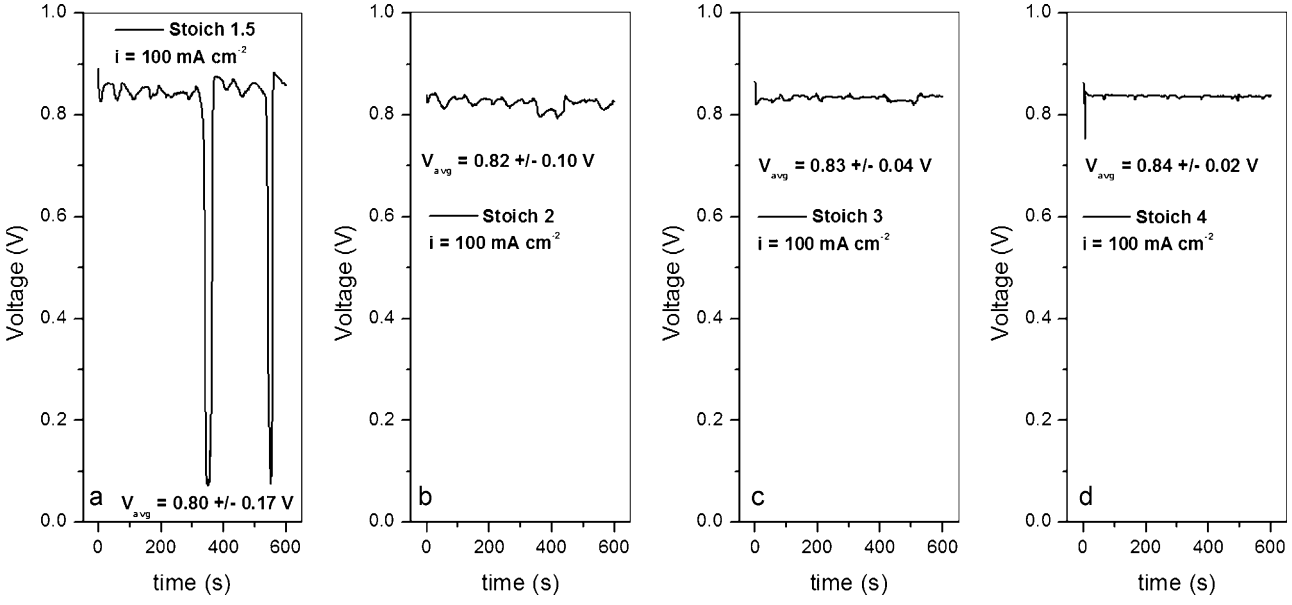

Fig. 7. Voltage signal at 100 mA cm^{-2} at (a) $\lambda_{air} = 1.5$; (b) $\lambda_{air} = 2$; (c) $\lambda_{air} = 3$; (d) $\lambda_{air} = 4$.

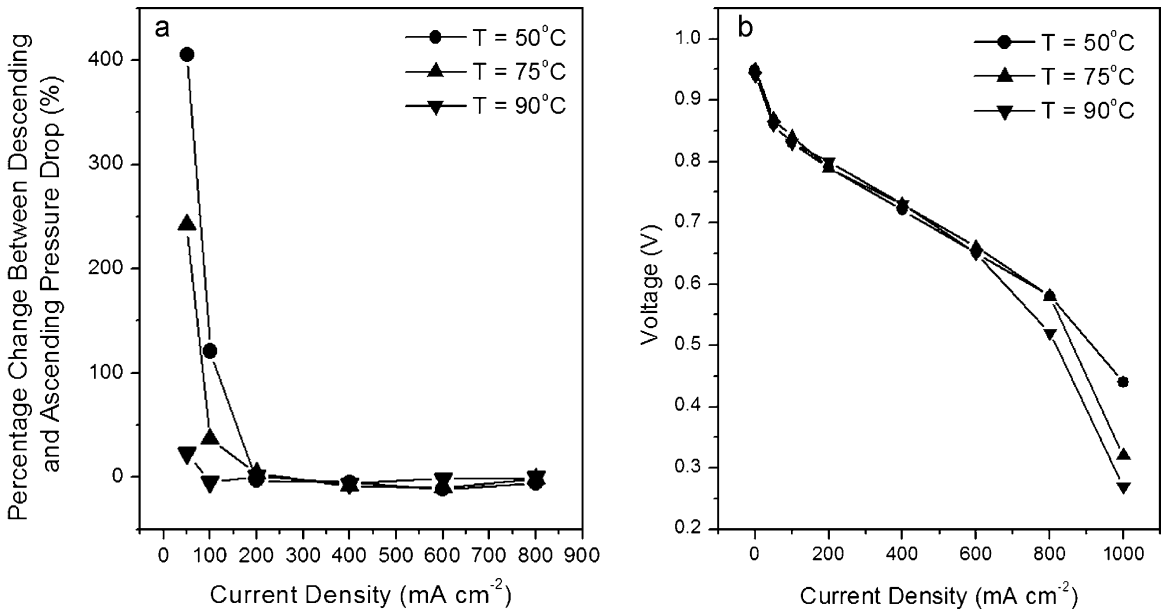

Fig. 8. (a) Percentage change between descending and ascending approaches for T = 50, 75, 90 °C and (b) ascending polarization curves for T = 50, 75, 90 °C.

removal abilities. The increased hysteresis at lower temperatures is also due to the increased condensation rates at lower temperature, resulting in more liquid water accumulation. Also, air at 90 °C can evaporate liquid water (if the RH drops below 100% locally) at a faster rate than 50 °C [29], which lessens the accumulation at higher temperatures. More liquid water present in the flow channels at lower operating temperatures also agrees with the work of Liu et al. [16] and Owejan et al. [28], who noted liquid water is a problem for automotive applications traveling short distances where lower temperature operation is expected.

As with the stoichiometry, the two-phase flow multiplier provides additional insight into the influence of the two-phase flow pressure drop. Fig. 9a and b shows the two-phase flow multiplier for the ascending and descending approaches, respectively, at 50, 75, and 90 °C. For all the temperatures during the ascending approach, the value of φ stays less than 2 and in some cases is approximately 1. This increase in pressure drop from the single-phase is caused by the two-phase flow resulting from the water breakthrough and humidified gas condensation. However, in the descending approach at these temperatures, additional water accumulates and increases the pressure drop, shown by the increased φ for current densities <400 mA cm^{-2}.

3.4. Effect of microporous layer (MPL)

Lu et al. [33] studied the breakthrough and two-phase flow characteristics of GDLs with and without a microporous layer. Their work shows that GDLs with an MPL exhibit lower GDL saturation and that the MPL promotes stable water paths with fewer water entry points into the GDL. Conversely, GDLs without

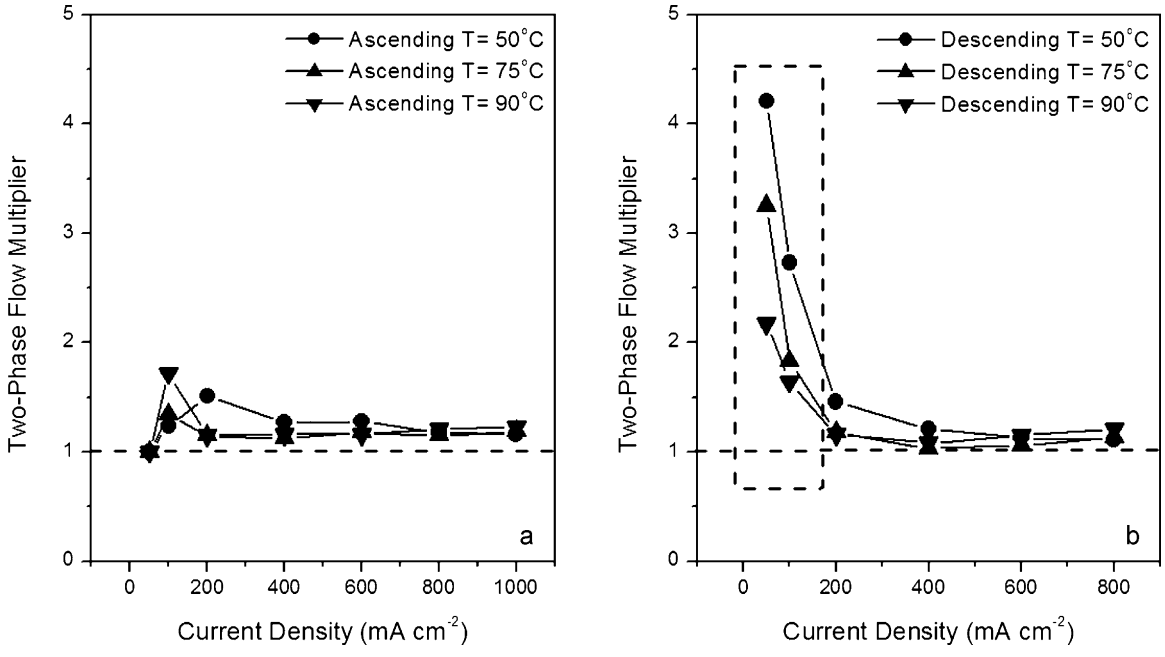

Fig. 9. Two-phase flow multiplier for T = 50–90 °C for (a) the ascending approach; (b) the descending approach.

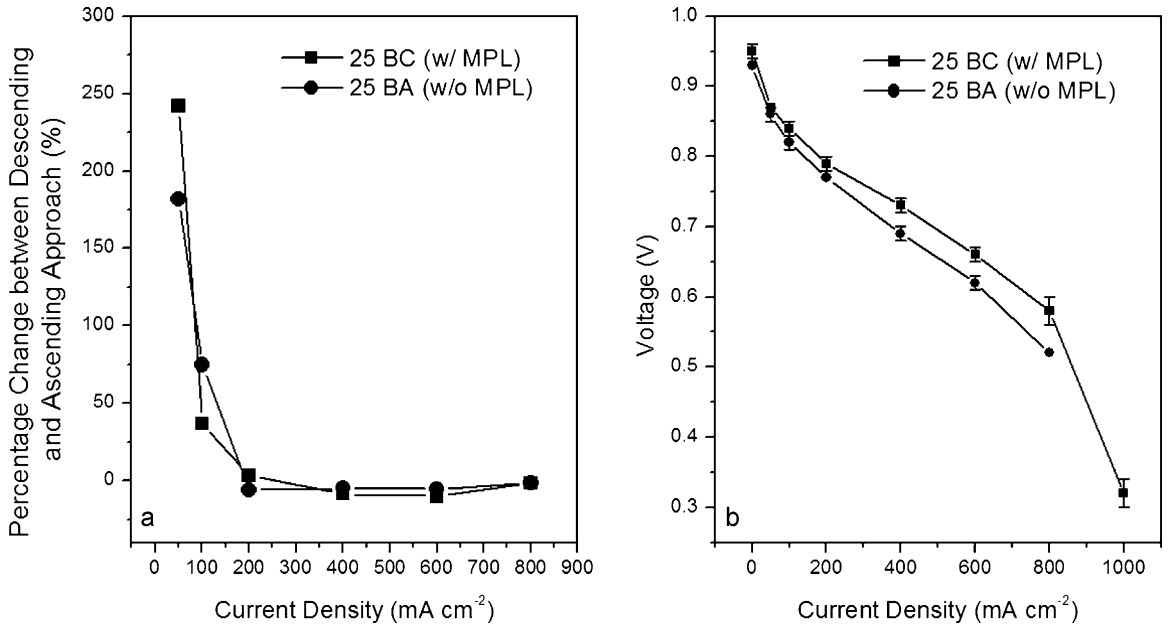

Fig. 10. Effect of MPL on (a) percentage change between descending and ascending pressure drop for 25 BC (MPL) and 25 BA (no MPL) and (b) polarization curves at baseline conditions for 25 BC (MPL) and 25 BA (no MPL).

an MPL exhibit greater saturation and dynamic breakthrough locations into the flow channels. The observed effect on two-phase flow in the flow channels was that GDLs without an MPL had more uniform water breakthrough over the GDL surface, leading to film flow on the channel walls, while the GDLs with an MPL tend toward the formation of slug flow.

The results for SGL 25 BC (with MPL) and SGL 25 BA (without MPL) on the cathode side are presented in Fig. 10. All other operating conditions are at the baseline conditions shown in Table 1. While the 25 BC GDL outperforms the 25 BA GDL electrochemically, which is consistent with the literature [20,21], there is no clear difference in the pressure drop hysteresis. The percentage change shows similar behavior between descending and ascending pressure drop for the two GDLs, with each GDL exhibiting hysteresis behavior at current densities <200 mA cm^{-2}.

With or without MPL, Fig. 11b shows both GDLs exhibit similar single-phase behavior (gas-phase only with no electrochemical reaction) and show similar ascending and descending pressure drop behavior. This result means that while the method of water injection may differ, the bulk influence of the liquid water on the two-phase flow pressure drop is similar. The similar influence of the two-phase flow is highlighted in Fig. 11a, where the two-phase flow multiplier is similar for either GDL for both the ascending and descending approach, with the major influence of the liquid water being consistently noted below <200 mA cm^{-2}. These results do not necessarily contradict the MPL influence/flow pattern developments discussed previously by Lu et al. [33] because for the superficial gas and liquid velocities in this work, our results are consistent with their flow pattern map, where slug flow is expected with either the 25 BC or 25 BA GDL. It should also be noted that those results were obtained with an ex situ apparatus (no electrochemical reaction, external water injection), and Lu et al. [33] pointed out that in situ results [31,34] have shown more droplets on the GDL surface due to water vapor being transported from the active catalyst layer through the MPL, which is consistent with this work.

4. Two-phase flow pressure drop prediction

While the single-phase pressure drop in laminar conditions is well predicted, the two-phase pressure drop relies on empirical approaches. The Lockhart–Martinelli (LM) approach is often used to predict the two-phase flow pressure drop. The LM approach uses a two-phase flow multiplier, which is the ratio of the two-phase pressure drop to the single-phase pressure drop as discussed in the experimental results (Eq. (3)). The two-phase multiplier is correlated to the Martinelli parameter, χ^2, which is defined by:

$$\chi^2 = \frac{\Delta P_l}{\Delta P_g} \tag{4}$$

Chisholm correlated φ_2 as a function of χ^2 with a constant, C, where C is a flow-regime dependant parameter.

$$\varphi_2 = 1 + C\chi + \chi^2 \tag{5}$$

For laminar liquids and gases, a value of $C = 5$ is typically used, though English and Kandlikar [35] modified C for non-circular minichannels.

However, Zhang et al. [36] found that this correlation did not match experimental data when permeable walls were considered. Thus, these correlations are not appropriate for fuel cells due to the porous GDL. To correct this problem, they proposed a variation of liquid water velocity along the channel, which should more closely resemble the actual water flow in a PEM fuel cell. This type of flow is shown in Fig. 12.

Assuming liquid is introduced continuously from a permeable wall, the pressure drop can be expressed as:

$$P_x - P_{x+dx} = \phi_2 \Delta P_g dx = (1 + C\chi + \chi^2)_x \Delta P_g dx \tag{6}$$

where the χ^2 parameter is determined by the local liquid velocity:

$$\chi^2|_x = \frac{u_L|_x \mu_L}{u_g \mu_g} \tag{7}$$

where μ refers to the viscosity and u refers to the velocity of the respective fluids. In theory, the liquid velocity should follow a linear relationship with the pressure difference assuming the water flowing through the porous media obeys Darcy's law. Integrating the above expression for a uniform and non-uniform (linear relationship with pressure) case, the expressions for the two-phase

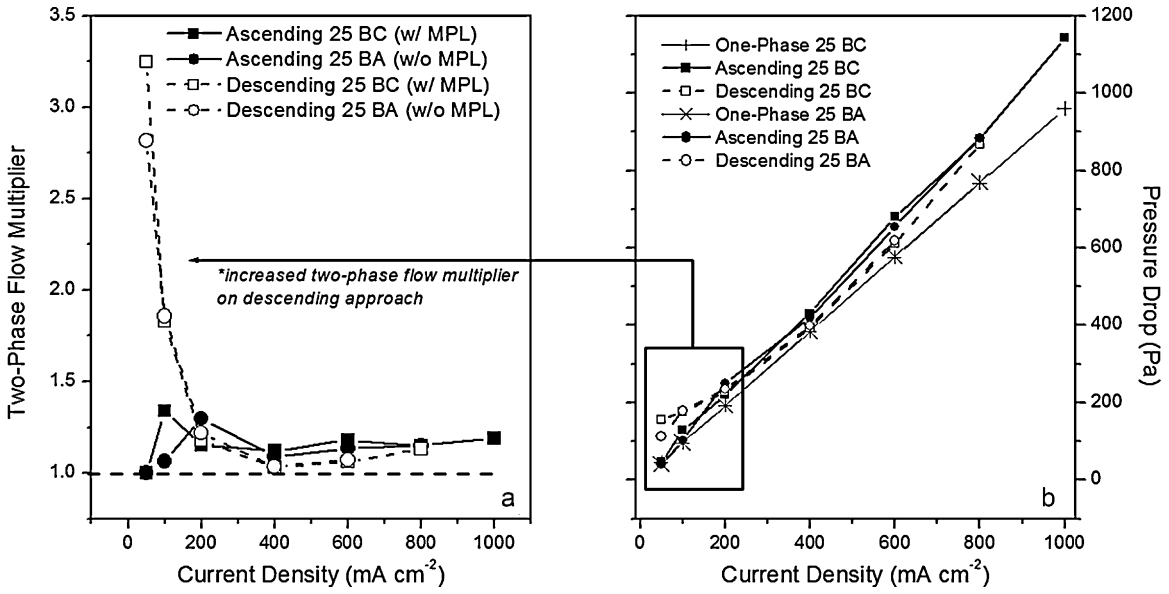

Fig. 11. Effect of MPL on (a) two-phase flow multiplier and (b) pressure drop hysteresis curves for 25 BA and 25 BC for single and two-phase flow.

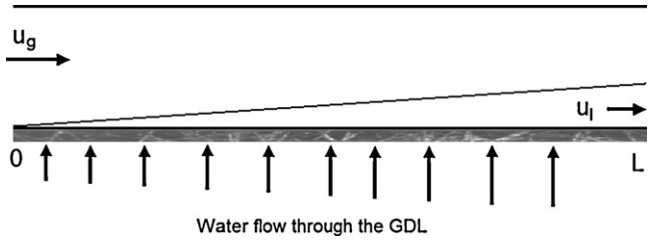

Fig. 12. Fuel cell water injection schematic showing water injection rate as a function of channel length.

pressure drop predications for both uniform and non-uniform injection are [37]:

$$\text{uniform}: \quad \Delta P_{gl} = \Delta P_g \left(1 + \left(\frac{2}{3}\right) C\chi + \left(\frac{1}{2}\right) \chi^2\right) \tag{8}$$

$$\text{non-uniform}: \quad \Delta P_{gl} = \Delta P_g \left(1 + \left(\frac{1}{2}\right) C\chi + \left(\frac{1}{3}\right) \chi^2\right) \tag{9}$$

The Martinelli parameter is particularly interesting in fuel cells because for a given set of conditions it is constant at every current density due to the coupling of the gas and liquid flow rates via Faraday's law. For typical fuel cell operating conditions, $\chi^2 < 0.1$. For the operating conditions studied during the electrochemically active hysteresis experiments ($T = 50$–$90\,^\circ$C, $\lambda_{air} = 1.5$–4), typical values were $\chi^2 < 0.02$. The results of this analysis are shown in Fig. 13 with the classic approach, uniform injection approach, and non-uniform injection approach highlighted. The two-phase flow multiplier presented here is the average multiplier at a given condition for the ascending approach, excluding the initial 50 mA cm^{-2} data point since this is confirmed as single-phase flow ($\varphi_{2\text{-phase}} = 1$). The liquid water velocity is calculated from the volumetric water production rate divided by the cross-sectional area of the channels, which assumes all product water enters the cathode channels.

There is some agreement between the data and the modified predictions for non-uniform and uniform water introduction. Generally, the classic approach over-predicts the data. The descending approach is currently neglected since the models do not take into account the additional accumulation of liquid water in the flow field channels during the descending approach, which greatly raises the experimental values of φ_2. While the prediction is satisfactory on the ascending approach, the model fails to capture all of the water transport phenomena occurring within the fuel cell. The assumption of all product water being removed via the cathode channels is not accurate, which would lower the Martinelli parameter. The flow of water back to the anode depends on several variables, so further refinement of the liquid water velocity is needed for a more accurate prediction. Also, the magnitude of the constant C may be optimized for fuel cell applications. These refinements and a prediction for the descending approach are the focus of upcoming work. These results illustrate a method to establish expected two-phase pressure drop values due to the unavoidable influence of liquid water in the fuel cell.

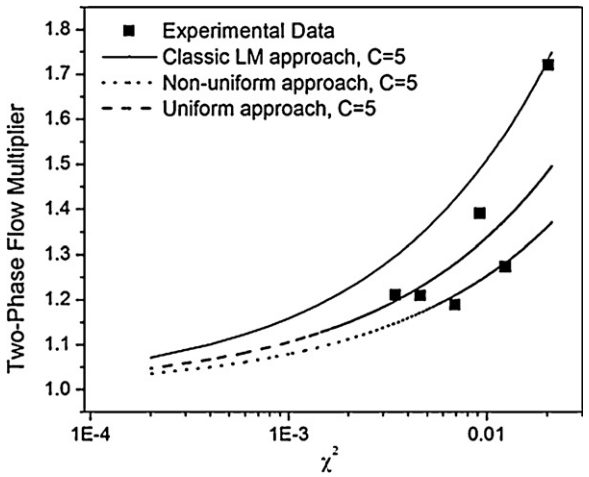

Fig. 13. Two-phase flow pressure drop prediction for the classic, non-uniform, and uniform approaches.

5. Conclusions

Two-phase flow pressure drop hysteresis occurs when the pressure drop differs depending on the path by which the current density is changed in an operating fuel cell. When the current density is increased, water from the electrochemical reaction and condensation of humidified reactants enters the flow field channels and causes the pressure drop to increase over the single-phase

pressure drop. However, when the current density is subsequently decreased, additional water accumulates in the flow field channels, causing the pressure drop at low current densities (generally <400 mA cm^{-2}) to be higher than both the single-phase and ascending two-phase pressure drop. The water accumulates further in the descending approach since the lower air flow rate cannot remove as much residual water (from the previous current density) convectively. This mechanism was confirmed with direct visual observation of the cathode flow field channels. Main observations include:

1. Increased air stoichiometry (in the range of 1.5–4) decreases the extent of the pressure drop hysteresis. This behavior occurs because the ability of the gas to convectively remove water increases with increased flow rate, causing the ascending and descending pressure drops to be the same. However, higher air flow rates cause the total magnitude of the pressure drop to increase.
2. Increased operating temperature (50–90 °C) decreases the extent of the pressure drop hysteresis. This result occurs because the increased air temperature increases the convective water removal capabilities of the gas and the condensation rate is lower at higher temperatures when fully humidified reactants are used. Conversely, lower temperatures increase the condensation rate, which increases the accumulation of liquid water on the descending approach.
3. The inclusion/exclusion of an MPL does not change the pressure drop hysteresis. Though the mechanism of water injection may differ, liquid water entering the channels increases the two-phase pressure drop in a similar manner due to the same flow patterns.
4. A modified Lockhart–Martinelli (LM) approach can be used to moderately predict the two-phase pressure drop hysteresis. The modification takes into account how liquid water enters the flow channels from a porous GDL wall, which leads to deviations from the classic LM approach. Further work is needed to predict the descending approach due to the accumulation of liquid water along this path.

Acknowledgements

Ryan Anderson is thankful for a graduate scholarship from the University of British Columbia. The authors are also grateful for continued collaboration with the National Research Council-Institute for Fuel Cell Innovation (NRC-IFCI) and the Automotive Fuel Cell Cooperation (AFCC).

References

[1] R. Anderson, L. Zhang, Y. Ding, M. Blanco, X. Bi, D.P. Wilkinson, J. Power Sources 195 (2010) 4531–4553.
[2] T.A. Trabold, Heat Transfer Eng. 26 (2005) 3–12.
[3] S.G. Kandlikar, Heat Transfer Eng. 29 (2008) 575–587.
[4] Z. Lu, A.D. White, J. Pelaez, M. Hardbarger, W. Domigan, J. Sergi, S.G. Kandlikar, Proceedings of the Sixth International ASME Conference on Nanochannels, Microchannels, and Minichannels, June 23–25, 2008.
[5] D. Spernjak, A.K. Prasad, S.G. Advani, J. Power Sources 195 (2010) 3553–3568.
[6] R. Anderson, D.P. Wilkinson, X. Bi, L. Zhang, J. Power Sources 195 (2010) 4168–4176.
[7] L.F. Zhang, H.T. Bi, D.P. Wilkinson, J. Stumper, H.J. Wang, J. Power Sources 183 (2008) 643–650.
[8] L.F. Zhang, W. Du, H.T. Bi, D.P. Wilkinson, J. Stumper, H.J. Wang, J. Power Sources 189 (2009) 1023–1031.
[9] R. Anderson, D.P. Wilkinson, X. Bi, L. Zhang, ECS Trans. 28 (2010) 127–137.
[10] S. Kundu, M. Cimenti, S. Lee, D. Bessarabov, Membr. Technol. (2009) 7–10.
[11] B. Li, R. Lin, D. Yang, J. Ma, Int. J. Hydrogen Energy 35 (2010) 2814–2819.
[12] E.S. Lee, C. Hidrovo, K. Goodson, J. Eaton, 6th International Conference on Multiphase Flow, Leipzig, Germany, 2007, Paper No. S7_Thu_A_46.
[13] D.P. Wilkinson, H.H. Voss, K. Prater, J. Power Sources 49 (1994) 117–127.
[14] Z. Lu, S.G. Kandlikar, C. Rath, M. Grimm, W. Domigan, A.D. White, M. Hardbarger, J.P. Owejan, T.A. Trabold, Int. J. Hydrogen Energy 34 (2009) 3445–3456.
[15] J. Dillet, O. Lottin, G. Maranzana, S. Didierjean, D. Conteau, C. Bonnet, J. Power Sources 195 (2010) 2795–2799.
[16] X. Liu, H. Guo, F. Ye, C.F. Ma, Int. J. Hydrogen Energy 33 (2008) 1040–1051.
[17] X. Liu, H. Guo, C.F. Ma, J. Power Sources 156 (2006) 267–280.
[18] X. Liu, H. Guo, F. Ye, C.F. Ma, Electrochim. Acta 52 (2007) 3607–3614.
[19] J.-H. Lin, W.-H. Chen, S.-H. Su, Y.-K. Liao, T.-H. Ko, J. Power Sources 184 (2008) 38–43.
[20] D. Spernjak, A.K. Prasad, S.G. Advani, J. Power Sources 170 (2007) 334–344.
[21] P. Owejan, T.A. Trabold, D.L. Jacobson, M. Arif, S.G. Kandlikar, Proceedings of the Fifth International Conference on Nanochannels, Microchannels, and Minichannels, Puebla, Mexico, 2007, pp. 407–408.
[22] F.-B. Weng, A. Su, C.-Y. Hsu, Int. J. Hydrogen Energy 32 (2007) 666–676.
[23] I.S. Hussaini, C.-Y. Wang, J. Power Sources 187 (2009) 444–451.
[24] E.C. Kumbur, K.V. Sharp, M.M. Mench, J. Power Sources 161 (2006) 333–345.
[25] US Fuel Cell Council, Protocol on Fuel Cell Component Testing: Primer for Generating Test Plans (USFCC 04-003A), 2006.
[26] J. Chen, J. Power Sources 195 (2010) 1122–1129.
[27] S. Basu, J. Li, C.-Y. Wang, J. Power Sources 187 (2009) 431–443.
[28] J.P. Owejan, J.J. Gagliardo, J.M. Sergi, S.G. Kandlikar, T.A. Trabold, Int. J. Hydrogen Energy 34 (2009) 3436–3444.
[29] N. Khajeh-Hosseini-Dalasm, K. Fusinobu, K. Okazaki, J. Power Sources 195 (2010) 7003–7010.
[30] E. Kimball, T. Whitaker, Y.G. Kevrekidis, J.B. Benziger, AIChE J. 54 (2008) 1313–1332.
[31] X.G Yang, F.Y. Zhang, A.L. Lubawy, C.Y. Wang, Electrochem. Solid State Lett. 7 (2004) A408–A411.
[32] A. Bazylak, J. Heinrich, N. Djilali, D. Sinton, J. Power Sources 185 (2008) 1147–1153.
[33] Z. Lu, M.M. Daino, C. Rath, S.G. Kandlikar, Int. J. Hydrogen Energy 35 (2010) 4222–4233.
[34] T. Ous, C. Arcoumanis, Int. J. Hydrogen Energy 34 (2009) 3476–3487.
[35] N. English, S.G. Kandlikar, Heat Transfer Eng. 27 (2006) 99–109.
[36] L. Zhang, X. Bi, D.P. Wilkinson, J. Stumper, H. Wang, 8th World Congress of Chemical Engineering, Montreal, Canada, August 24–27, 2009, pp. 1–6, Paper No. 145.
[37] L. Zhang, X.T. Bi, D.P. Wilkinson, R. Anderson, J. Stumper, H. Wang, Chem. Eng. Sci., 2011, doi:10.1016/j.ces.2011.01.030.